Topological semimetals with Riemann surface states

Chen Fang*†[1,2], Ling Lu†[1], Junwei Liu[1] and Liang Fu*[1]
[1] *Department of physics, Massachusetts Institute of Technology, Cambridge, MA 02139, USA and*
[2] *Beijing National Laboratory for Condensed Matter Physics, and Institute of Physics, Chinese Academy of Sciences, Beijing 100190, China**

(Dated: December 8, 2015)

Riemann surfaces are geometric constructions in complex analysis that may represent multi-valued holomorphic functions using multiple sheets of the complex plane. We show that the energy dispersion of surface states in topological semimetals can be represented by Riemann surfaces generated by holomorphic functions in the two-dimensional momentum space, whose constant height contours correspond to Fermi arcs. This correspondence is demonstrated in the recently discovered Weyl semimetals and leads us to predict new types of topological semimetals, whose surface states are represented by double- and quad-helicoid Riemann surfaces. The intersection of multiple helicoids, or the branch cut of the generating function, appears on high-symmetry lines in the surface Brillouin zone, where surface states are guaranteed to be doubly degenerate by a glide reflection symmetry. We predict the heterostructure superlattice $[(SrIrO_3)_2(CaIrO_3)_2]$ to be a topological semimetal with double-helicoid Riemann surface states.

Introduction The study of topological semimetals[1] has seen rapid progress since the theoretical proposal of a three-dimensional Weyl semimetal in a magnetic phase of pyrochlore iridates[2]. In general, topological semimetals are materials where the conduction and the valence bands cross in the Brillouin zone and the crossing cannot be removed by perturbations preserving certain crystalline symmetry such as the lattice translation. Bloch states in the vicinity of the band crossing possess a nonzero topological index, e.g., the Chern number in case of Weyl semimetals. The nontrivial topology gives rise to anomalous bulk properties of topological semimetals such as the chiral anomaly[3–5]. Several classes of topological semimetals have been theoretically proposed so far, including Weyl,[2, 6–13], Dirac[14–17] and nodal line semimetals[7, 17–30], some among which have been experimentally observed[31–47].

Surface states of topological semimetals have attracted much attention. On the surface of a Weyl semimetal, the Fermi surface consists of open arcs connecting the projection of bulk Weyl points onto the surface Brillouin zone [2], instead of closed loops. The presence of Fermi arcs on the surface is a remarkable property that directly reflects the nontrivial topology of the bulk, and plays a key role in the experimental identification of Weyl semimetals[32, 33, 36]. In contrast, as shown by recent theoretical works[18, 21, 23, 24, 28, 48, 49], existing Dirac and nodal line semimetals do *not* have robust Fermi arcs that are stable against symmetry-allowed perturbations. Therefore, the general condition for protected Fermi arcs and their existence in topological semimetals beyond Weyl remain open questions.

In this work, we report the discovery of a new topological semimetal phase in a wide variety of nonsymmorphic crystal structures with the glide reflection symmetry, a combination of a reflection and a translation. Such nonsymmorphic topological semimetals have either Dirac points or Weyl dipoles in the bulk, which are associated with a Z_2 topological invariant that we define. These band crossing points are pairwise connected by symmetry-protected Fermi arcs on the surface, with a unique connectivity determined by the Z_2 topological charge. Interestingly, these surface states have a momentum-energy dispersion that can be mapped to the Riemann surface for a holomorphic function whose singularity corresponds to the bulk Dirac or Weyl points, and hence dubbed "Riemann surface states". By relating the Z_2 topological index to rotation eigenvalues of energy bands, we provide a simple criterion for the nonsymmorphic topological semimetal phase and predict its material realization in the recently synthesized superlattice heterostructure of iridates[50] $[(SrIrO_3)_{2m}(CaIrO_3)_{2n}]$.

Weyl semimetal and Riemann surface We start by considering the energy-momentum relation $E(\mathbf{k}_\parallel)$ of surface states of Weyl semimetals, where $\mathbf{k}_\parallel$ is the surface momentum. $E(\mathbf{k}_\parallel)$ is bounded by the conduction and valence band edges in the bulk cones [see the head-to-head cones in Fig.1(a)], obtained by collapsing energies of bulk states with the same $\mathbf{k}_\parallel$ at different perpendicular momenta k_z. In the most generic case, we assume that there be N_s surface bands, $E_1(\mathbf{k}_\parallel) < E_2(\mathbf{k}_\parallel) < ... < E_{N_s}(\mathbf{k}_\parallel)$. Consider a loop in the surface Brillouin zone enclosing the projection of the Weyl point. The Chern number of the Weyl point dictates that[2], as a $\mathbf{k}$-point moves one round along the loop counterclockwise (clockwise), the energy of the state does not return to the same value, but moves one band higher (lower), that is, $E_n(\mathbf{k}_\parallel) \to E_{n+1}(\mathbf{k}_\parallel)$ $[E_n(\mathbf{k}_\parallel) \to E_{n-1}(\mathbf{k}_\parallel)]$. As $\mathbf{k}_\parallel$ keeps circling the loop counterclockwise (clockwise), the band index keeps increasing (decreasing) before the state merges into the conduction (valence) bulk. In this process, the dispersion along the loop maps out a spiral that connects the two bulk cones, and as one sweeps the radius of the loop, the spirals at different radii form a helicoid as shown in

* fangc@mit.edu; liangfu@mit.edu
† The first two authors contributed equally to this work.

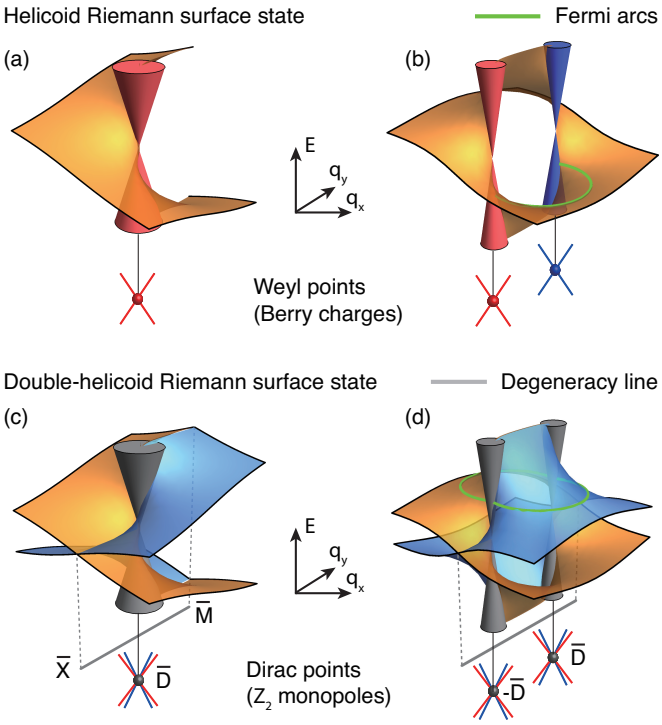

FIG. 1. (a) The surface dispersion near the projection of a Weyl point with Chern number +1, where the red solid cones are the projection of the bulk states and the helicoid sheet represents the surface states. This is also the Riemann surface of Im[log(q)]. (b) The surface dispersion near the projections of a pair of Weyl points with opposite Chern numbers, where the red and the blue cones represent the bulk states projection, and the green contour is an iso-energy contour also known as a Fermi arc. This is also the Riamann surface of Im[log $\frac{q-k_1}{q-k_2}$]. (c) The surface dispersion of the nonsymmorphic Dirac semimetal near the Dirac point, where the gray cones represent the projection of bulk states. This is also the Riemann surface of the function given in Eq.(4) in the text. (d) The surface dispersion near two nonsymmorphic Dirac points, with iso-energy contours of two Fermi arcs.

Fig.1(a).

The winding of the energy dispersion along any loop enclosing the Weyl point is the same as the winding of the phase of a holomorphic function along any loop enclosing a simple (linear order) zero. Near a simple zero, a general holomorphic function takes the form $f(z) = z - z_0 + O[(z-z_0)^2]$ up to an overall factor. As z goes around z_0 counterclockwise (clockwise), the phase of $f(z)$ increases (decreases) by 2π. Therefore, the phase of $f(z)$ near z_0, or the imaginary part of $\log[f(z)]$, is topologically equivalent to the dispersion of the surface states near the projection of a positive Weyl point. Similarly, one can show that the phase of a holomorphic function near a simple pole is equivalent to the energy dispersion near the projection of a negative Weyl point. This topological equivalence can be expressed as

$$E(\mathbf{q}_{\|}) \sim \mathrm{Im}[\log(q^{\pm 1})], \qquad (1)$$

where $\mathbf{q}_{\|}$ is the surface momentum relative to the Weyl point projection and $q = q_a + iq_b$, and ± 1 corresponds to Weyl point of positive and negative monopole charge. There is one caveat in understanding Eq.(1): while the function on the right-hand-side ranges from negative to positive infinity, the energy of the surface bands always merge into the bulk. This infinite winding of the surface dispersion implies that the theory cannot be made ultraviolet-complete in 2D, but is only consistent for the surface states of some topologically nontrivial 3D bulk: a demonstration of the bulk-edge correspondence principle in Weyl semimetals.

In complex analysis, the plot of the real or the imaginary part of a multi-valued holomorphic (meromorphic) function is called a Riemann surface, which is a surface-like configuration that covers the complex plane a finite (compact) or infinite (noncompact) number of times[51]. Eq.(1) establishes the topological equivalence between the surface dispersion of a Weyl semimetal and a *non-compact* Riemann surface. Both share the following characteristic feature: There is no equal energy (equal height) contour that is both closed and encloses the projection of the Weyl point, a feature that directly leads to the phenomenon of "Fermi arcs". This topological equivalence can be extended to the case of multiple Weyl points. If there are two Weyl points' projections at (k_{1a}, k_{1b}) and (k_{2a}, k_{2b}), then the corresponding function is simply $\log[(q-k_1)(q-k_2)^{-1}]$, where $k_i = k_{ia} + ik_{ib}$, whose imaginary part is plotted in Fig.1(b). Cutting the dispersion at any energy, the iso-energy contour is an arc connecting $\mathbf{k}_1$ and $\mathbf{k}_2$.

Double-helicoid Riemann surface state protected by one glide reflection symmetry in a Dirac semimetal A Dirac point can be considered as the superposition of two Weyl points with opposite Chern numbers[14, 15], the same way the 3D massless Dirac equations decouple into two sets of Weyl equations[52]. The surface states near the projection of a Dirac point is hence a superposition of a helicoid and an anti-helicoid Riemann surface as shown in Fig.1(c), which cross each other along certain lines, and may have two Fermi arcs[15, 16, 45]. Yet, if there be no additional symmetry that protects their crossing, hybridization along the crossing lines opens a gap and the double-helicoid structure of the surface dispersion is lost and the Fermi arcs also disappear. This has been the case of all Dirac semimetals discovered so far. Below we show that a nonsymmorphic symmetry[29, 53–61] protects the crossing and with it the topological surface states.

Consider a three-dimensional system with the following symmetries: a glide reflection, G, that reverses the a-direction then translates by half lattice constant along the b-direction, and time-reversal symmetry, T. Define the antiunitary symmetry Θ as their composition

$$\Theta \equiv G * T : \ (x, y, z, t) \to (-x, y + 1/2, z, -t), \qquad (2)$$

where (x, y, z) are the spatial coordinates along a, b, c-axes in unit of the corresponding lattice constants. Eq.(2)

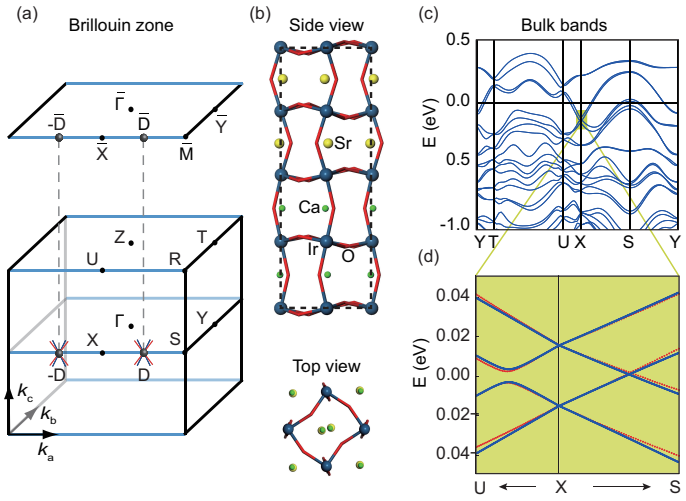

FIG. 2. (a) The Brillouin zone and the (001)-slab surface Brillouin zone of a orthorhombic lattice with a glide reflection, where the lines of double degeneracy are marked in blue and the Dirac points and their projections are marked by green dots. (b) One unit cell of heterostructure superlattice $[(SrIrO_3)_{2m}(CaIrO_3)_{2n}]$ with $m = n = 1$. (c) The bulk band structure of the superlattice along the path YTUXSY, calculated from first principles. (d) The zoomed-in band structure of the same system near X, where the first principles results (red dots) are fitted using a tight-binding model modified from Ref.[27] (blue line).

implies that the momentum of a single quasiparticle, (k_a, k_b, k_c), is sent to $(k_a, -k_b, -k_c)$. Importantly, the square of Θ

$$\Theta^2 = G^2T^2 = T_{010} = e^{-ik_b}, \tag{3}$$

where T_{010} is the unit lattice translation along the b-direction. Specially at the Brillouin zone boundary $k_b = \pi$, we have $\Theta^2 = -1$. This leads to double degeneracy of all states on two high-symmetry lines, UR and XS, analogous to the well-known Kramers' degeneracy[62] [blue lines in the 3D Brillouin zone of Fig. 2(a)], with the key difference that the latter leads to double degeneracy at high-symmetry points in a spinful system, Θ leads to double degeneracy along the whole high-symmetry lines in both spinful and spinless systems.

Then we consider the states on the (001)-surface. In the surface Brillouin zone, Eq.(3) leads to double degeneracy along $\bar{X}\bar{M}$ [blue line in the surface Brillouin zone of Fig. 2(a)]. This degeneracy is exactly what is needed to protect the double-helicoid surface states shown in Fig.1(c): if there is a projection of Dirac point on $\bar{X}\bar{M}$ and the two helicoids intersect along $\bar{X}\bar{M}$, the symmetry guaranteed double degeneracy disallows their hybridization. In the double-helicoid dispersion, each iso-energy contour must contain two arcs emanating from the projection of the Dirac point. Due to time-reversal, each projection of Dirac point at $\bar{D}$ is accompanied by one at $-\bar{D}$. The surface dispersion with two Dirac points is shown in Fig.1(d), and each iso-energy contour must contain two arcs connecting $\bar{D}$ and $-\bar{D}$.

As the surface dispersion near a Weyl point projection can be mapped to the Riemann surface of $\log(z)$, a natural question is if the the surface dispersion of the Dirac semimetals can also be mapped to some Riemann surface representing a holomorphic function. Configuration of two surfaces crossing along certain lines reminds us of Riemann surfaces of holomorphic functions involving a fractional power. For example, $f(z) = \sqrt{z^2}$ has two branches $f_\pm(z) = \pm z$, and the imaginary parts of the two branches meet each other at the real axis, as $\mathrm{Im}(z) = \mathrm{Im}(-z) = 0$ for $z \in \mathbb{R}$. Since the dispersion near the positive and the negative Weyl points are mapped to the phases of z and z^{-1}, what we are looking for is a homomorphic function whose two branches are $\log z$ and $\log z^{-1}$. These considerations suggest the following choice

$$E(\mathbf{q}_\parallel) \sim \mathrm{Im}[\log(q + q^{-1} + \sqrt{q^2 + q^{-2} - 2})], \tag{4}$$

where $\mathbf{q} = \mathbf{k} - \bar{\mathrm{D}}$.

According to the bulk-edge correspondence principle, the nontrivial surface state protected by Θ suggests a nontrivial bulk topology near each Dirac point. In the main text, for concision, we only make the following remarks and leave the detailed discussion of bulk topology to the Supplemental Materials: (i) A Dirac point is either on XS or UR; (ii) On a sphere enclosing the Dirac point, there is a Z_2 topological invariant protected by Θ; (iii) if inversion is also present and if the system is spinful (with SOC), the invariant can be expressed in terms of rotation eigenvalues of bands along XS or UR, analogous to the Fu-Kane formula for topological insulators[63]. In the absence of additional symmetry but only Θ, the Dirac point is not protected and is split into two Weyl points of opposite charge along XS or UR, termed a Weyl dipoles, related to each other by Θ. In this case, we consider a sphere enclosing the Weyl dipoles. The Chern number of the sphere is zero due to the cancelation of monopole charge, but the new Z_2 topological charge is nontrivial. In this case, on the surface, Fermi arcs only connect Weyl points from *different* Weyl dipoles, and the two Weyl points within one Weyl dipole are not connected by any Fermi arc.

Material realization in iridates Perovskite iridate $SrIrO_3$ was shown to be a TSM with a degenerate nodal line protected by a twofold screw axis[27, 29]. It was found in Ref.[27] that if a staggering chemical potential propagating along the [001]-direction, the nodal line is gapped at all but two points. Based on this finding, we propose to realize the nonsymmorphic Dirac semimetal in a $[(SrIrO_3)_{2m}(CaIrO_3)_{2n}]$ superlattice heterostructure shown in Fig.2(b). For $m = n = 1$, we perform a first principles calculation for the bulk band structure, and find a pair of Dirac points along XS that are close and symmetric on each side of X shown in Fig.2(c). We modify the tight-binding model given in Ref.[27] such that its band structure quantitatively matches that from the first principles calculation near X [Fig.2(d)]. (Also find

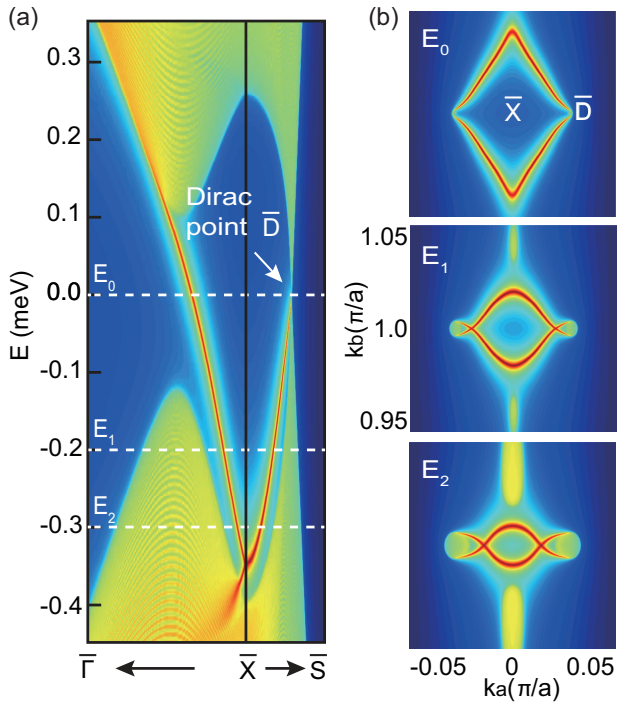

FIG. 3. (a) The spectral weight of the top surface of a (001)-slab, along the path $\bar{\Gamma}$-$\bar{X}$-$\bar{M}$, calculated from the tight-binding model used in fitting. (b) The spectral weight of the (001)-surface at, from top to bottom, $E_{0,1,2}$ respectively.

details of the tight-binding model in Supplementary Materials.) Using the fitted tight-binding model, we calculated the spectral weight of the states near the top surface of a (001)-slab, along high-symmetry lines in surface Brillouin zone [Fig.3(a)], and the 2D surface Brillouin zone near $\bar{X}$ at three different energies [Fig.3(b)], where the double Fermi arcs can be seen. We note that as the energy decreases from E_0, the energy of the bulk Dirac point, (i) bulk pockets emerge near the projection of the Dirac point and (ii) more importantly, the configuration of the two arcs rotation around the projections of the Dirac points, such that in Fig.3(b), the two arcs cross each other along $\bar{X}\bar{M}$, where the crossing point is always protected by Θ.

Quad-helicoid surface state protected by two glide reflections Finally, we point out that new types of TSM may exist if additional nonsymmorphic symmetries on the surface are present, with their own characteristic surface dispersions. As an example, we assume there be an additional glide plane, G', that is perpendicular to G,

$$G' : (x, y, z) \to (x + 1/2, -y, z). \tag{5}$$

Following similar steps, we find that $\Theta' \equiv G' * T$ guarantees double degeneracy along $\bar{Y}\bar{M}$, so that if both Θ and Θ' are present, all bands are doubly degenerate along $\bar{X}\bar{M}$ and $\bar{Y}\bar{M}$. This double degeneracy protects a unique nontrivial surface dispersion consisting of four spiral surfaces near $\bar{M}$, as shown in Fig. 4, or can be considered as the superposition of the surface dispersions near four

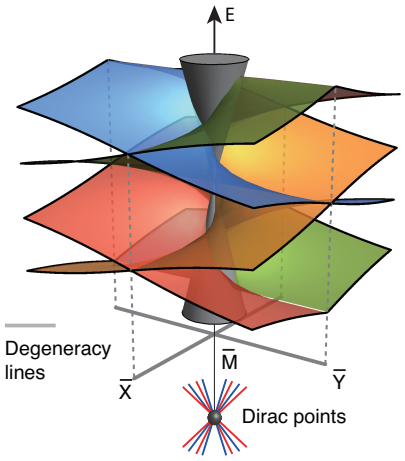

FIG. 4. The quad-helicoid surface state dispersion, consisting of two helicoids (blue and red) and two anti-helicoids (green and yellow). The blue and the green, and the yellow and the red cross each other along $\bar{M}\bar{X}$, and the blue and the yellow and the red and the green cross each other along $\bar{M}\bar{Y}$.

Weyl points, two positive and two negative ones. This dispersion has a new type of Z_2 spectral flow between two perpendicular lines of $\bar{X}\bar{M}$ and $\bar{Y}\bar{M}$: two bands from a degenerate pair at $\bar{X}\bar{M}$ flow to different degenerate pairs at $\bar{Y}\bar{M}$. A generic iso-energy contour of this quad-helicoid surface dispersion consists of four Fermi arcs emanating from $\bar{M}$. Since there is only one $\bar{M}$ inside the surface Brillouin zone, we argue that no topological invariant can be defined for the band crossings which project to $\bar{M}$, or the Nielson-Ninomiya theorem would be violated. We conjecture that the system belongs to filling enforced semimetals discussed in Ref.[53 and 59], where the band crossings are guaranteed by the space group at certain integer fillings. In this case, the surface dispersion can also be mapped to a Riemann surface. Since the dispersion can be considered as the superposition of four spiral surfaces, we consider a holomorphic function with four branches. Θ and Θ' require that two branches meet along $\bar{X}\bar{M}$ (defined as the real axis) and $\bar{Y}\bar{M}$ (defined as the imaginary axis), respectively. The function we choose is

$$E(\mathbf{q}_{\|}) \sim \mathrm{Im}[\log(\sqrt{q^2 + q^{-2} + 2} + \sqrt{q^2 + q^{-2} - 2})], \tag{6}$$

where $q = (k_a - \pi) + i(k_b - \pi)$

Conclusions In this paper we theoretically find two new classes of topological semimetals that have multiple Fermi arcs on the surface protected by nonsymmorphic glide reflections symmetries and time-reversal. We observe that so far, all topological semimetals with protected Fermi arcs have surface dispersions that are topologically equivalent to the noncompact Riemann surfaces representing simple holomorphic functions. We propose superlattice heterostructure $[(SrIrO_3)_{2m}(CaIrO_3)_{2n}]$ as a nonsymmorphic Dirac semimetal with two Fermi arcs on the (001)-plane protected by one glide reflection.

Acknowledgements We thank Timothy H. Hsieh

for discussion. C.F. thanks Yige Chen for helpful discussion on the tight-binding model. C.F. thanks Jian Liu for fruitful discussions on potential material systems. C.F. and L.F. were supported by S3TEC Solid State Solar Thermal Energy Conversion Center, an Energy Frontier Research Center funded by the U.S. Department of Energy (DOE), Office of Science, Basic Energy Sciences (BES), under Award No. de-sc0001299/DE-FG02-09ER46577. L.L. was supported in part by U.S.A.R.O. through the ISN under Contract No. W911NF-13-D-0001, in part by the MRSEC Program of the NSF under Award No. DMR-1419807, and in part by the MIT S3TEC EFRC of DOE under Grant No.DESC0001299. J. L was supported by the STC Center for Integrated Quantum Materials, NSF Grant No. DMR-1231319.

[1] Shuichi Murakami, "Phase transition between the quantum spin hall and insulator phases in 3d: emergence of a topological gapless phase," New Journal of Physics **9**, 356 (2007).

[2] Xiangang Wan, Ari M. Turner, Ashvin Vishwanath, and Sergey Y. Savrasov, "Topological semimetal and Fermi-arc surface states in the electronic structure of pyrochlore iridates," Phys. Rev. B **83**, 205101 (2011).

[3] Pavan Hosur, S. A. Parameswaran, and Ashvin Vishwanath, "Charge transport in weyl semimetals," Phys. Rev. Lett. **108**, 046602 (2012).

[4] D. T. Son and B. Z. Spivak, "Chiral anomaly and classical negative magnetoresistance of weyl metals," Phys. Rev. B **88**, 104412 (2013).

[5] Chao-Xing Liu, Peng Ye, and Xiao-Liang Qi, "Chiral gauge field and axial anomaly in a weyl semimetal," Phys. Rev. B **87**, 235306 (2013).

[6] A. A. Burkov, M. D. Hook, and Leon Balents, "Topological nodal semimetals," Phys. Rev. B **84**, 235126 (2011).

[7] A. A. Burkov and Leon Balents, "Weyl semimetal in a topological insulator multilayer," Phys. Rev. Lett. **107**, 127205 (2011).

[8] Gang Xu, Hongming Weng, Zhijun Wang, Xi Dai, and Zhong Fang, "Chern semimetal and the quantized anomalous hall effect in hgcr$_2$se$_4$," Phys. Rev. Lett. **107**, 186806 (2011).

[9] Chen Fang, Matthew J. Gilbert, Xi Dai, and B. Andrei Bernevig, "Multi-weyl topological semimetals stabilized by point group symmetry," Phys. Rev. Lett. **108**, 266802 (2012).

[10] Ling Lu, Liang Fu, John D. Joannopoulos, and Marin Soljacic, "Weyl points and line nodes in gyroid photonic crystals," Nature Photonics (2013).

[11] Hongming Weng, Chen Fang, Zhong Fang, B. Andrei Bernevig, and Xi Dai, "Weyl semimetal phase in noncentrosymmetric transition-metal monophosphides," Phys. Rev. X **5**, 011029 (2015).

[12] Shin-Ming Huang, Su-Yang Xu, Ilya Belopolski, Chi-Cheng Lee, Guoqing Chang, BaoKai Wang, Nasser Alidoust, Guang Bian, Madhab Neupane, Arun Bansil, *et al.*, "An inversion breaking weyl semimetal state in the taas material class," Nature Communications **6** (2015).

[13] Alexey A. Soluyanov, Dominik Gresch, Zhijun Wang, QuanSheng Wu, Matthias Troyer, Xi Dai, and B. Andrei Bernevig, "A new type of weyl semimetals," arXiv:1507.01603 (2015).

[14] S. M. Young, S. Zaheer, J. C. Y. Teo, C. L. Kane, E. J. Mele, and A. M. Rappe, "Dirac semimetal in three dimensions," Phys. Rev. Lett. **108**, 140405 (2012).

[15] Zhijun Wang, Yan Sun, Xing-Qiu Chen, Cesare Franchini, Gang Xu, Hongming Weng, Xi Dai, and Zhong Fang, "Dirac semimetal and topological phase transitions in A(3)Bi (A = Na, K, Rb)," Phys. Rev. B **85**, 195320 (2012).

[16] Zhijun Wang, Hongming Weng, Quansheng Wu, Xi Dai, and Zhong Fang, "Three-dimensional dirac semimetal and quantum transport in cd$_3$as$_2$," Phys. Rev. B **88**, 125427 (2013).

[17] Minggang Zeng, Chen Fang, Guoqing Chang, Yu-An Chen, Timothy Hsieh, Arun Bansil, Hsin Lin, and Liang Fu, "Topological semimetals and topological insulators in rare earth monopnictides," arXiv:1504.03492 (2015).

[18] Ching-Kai Chiu and Andreas P. Schnyder, "Classification of reflection-symmetry-protected topological semimetals and nodal superconductors," Phys. Rev. B **90**, 205136 (2014).

[19] Michael Phillips and Vivek Aji, "Tunable line node semimetals," Phys. Rev. B **90**, 115111 (2014).

[20] Kieran Mullen, Bruno Uchoa, and Daniel T. Glatzhofer, "Line of dirac nodes in hyperhoneycomb lattices," Phys. Rev. Lett. **115**, 026403 (2015).

[21] Hongming Weng, Yunye Liang, Qiunan Xu, Rui Yu, Zhong Fang, Xi Dai, and Yoshiyuki Kawazoe, "Topological node-line semimetal in three-dimensional graphene networks," Phys. Rev. B **92**, 045108 (2015).

[22] Lilia S. Xie, Leslie M. Schoop, Elizabeth M. Seibel, Quinn D. Gibson, Weiwei Xie, and Robert J. Cava, "A new form of ca3p2 with a ring of dirac nodes," APL Materials **3**, 083602 (2015).

[23] Youngkuk Kim, Benjamin J. Wieder, C. L. Kane, and Andrew M. Rappe, "Dirac line nodes in inversion-symmetric crystals," Phys. Rev. Lett. **115**, 036806 (2015).

[24] Rui Yu, Hongming Weng, Zhong Fang, Xi Dai, and Xiao Hu, "Topological node-line semimetal and dirac semimetal state in antiperovskite cu$_3$PdN," Phys. Rev. Lett. **115**, 036807 (2015).

[25] Jun-Won Rhim and Yong Baek Kim, "Landau level quantization and almost flat modes in three-dimensional semimetals with nodal ring spectra," Phys. Rev. B **92**, 045126 (2015).

[26] Ching-Kai Chiu, Jeffrey C.Y. Teo, Andreas P. Schnyder, and Shinsei Ryu, "Classification of topological quantum matter with symmetries," arXiv:1505.03535 (2015).

[27] Jean-Michel Carter, V. Vijay Shankar, M. Ahsan Zeb, and Hae-Young Kee, "Semimetal and topological insulator in perovskite iridates," Phys. Rev. B **85**, 115105 (2012).

[28] Yige Chen, Yuan-Ming Lu, and Hae-Young Kee, "Topological crystalline metal in orthorhombic perovskite iridates," Nature Communications **6** (2015).

[29] Chen Fang, Yige Chen, Hae-Young Kee, and Liang

Fu, "Topological nodal line semimetals with and without spin-orbital coupling," Phys. Rev. B **92**, 081201 (2015).
[30] Jeffrey G Rau, Eric Kin-Ho Lee, and Hae-Young Kee, "Spin-orbit physics giving rise to novel phases in correlated systems: Iridates and related materials," arXiv preprint arXiv:1507.06323 (2015).
[31] Ling Lu, Zhiyu Wang, Dexin Ye, Lixin Ran, Liang Fu, John D. Joannopoulos, and Marin Soljacic, "Experimental observation of weyl points," Science **349**, 622 (2015).
[32] Su-Yang Xu, Ilya Belopolski, Nasser Alidoust, Madhab Neupane, Chenglong Zhang, Raman Sankar, Shin-Ming Huang, Chi-Cheng Lee, Guoqing Chang, BaoKai Wang, Guang Bian, Hao Zheng, Daniel S. Sanchez, Fangcheng Chou, Hsin Lin, Shuang Jia, and M. Zahid Hasan, "Experimental realization of a topological weyl semimetal phase with fermi arc surface states in taas," Science **349**, 613 (2015).
[33] B. Q. Lv, H. M. Weng, B. B. Fu, X. P. Wang, H. Miao, J. Ma, P. Richard, X. C. Huang, L. X. Zhao, G. F. Chen, Z. Fang, X. Dai, T. Qian, and H. Ding, "Experimental discovery of weyl semimetal taas," Phys. Rev. X **5**, 031013 (2015).
[34] Chandra Shekhar, Ajaya K. Nayak, Yan Sun, Marcus Schmidt, Michael Nicklas, Inge Leermakers, Uli Zeitler, Yurii Skourski, Jochen Wosnitza, Zhongkai Liu, Yulin Chen, Walter Schnelle, Horst Borrman, Yuri Grin, Claudia Felser, and Binghai Yan, "Extremely large magnetoresistance and ultrahigh mobility in the topological weyl semimetal candidate nbp," Nature Physics **11**, 645 (2015).
[35] B. Q. Lv, N. Xu, H. M. Weng, J. Z. Ma, P. Richard, X. C. Huang, L. X. Zhao, G. F. Chen, C. E. Matt, F. Bisti, V. N. Strocov, J. Mesot, Z. Fang, X. Dai, T. Qian, M. Shi, and H. Ding, "Observation of weyl nodes in taas," Nature Physics **11**, 724 (2015).
[36] L. X. Yang, Z. K. Liu, Y. Sun, H. Peng, H. F. Yang, T. Zhang, B. Zhou, Y. Zhang, Y. F. Guo, M. Rahn, D. Prabhakaran, Z. Hussain, S.-K. Mo, C. Felser, B. Yan, and Y. L. Chen, "Weyl semimetal phase in the noncentrosymmetric compound taas," Nature Physics **11**, 728 (2015).
[37] Su-Yang Xu, Nasser Alidoust, Ilya Belopolski, Zhujun Yuan, Guang Bian, Tay-Rong Chang, Hao Zheng, Vladimir N. Strocov, Daniel S. Sanchez, Guoqing Chang, Chenglong Zhang, Daixiang Mou, Yun Wu, Lunan Huang, Chi-Cheng Lee, Shin-Ming Huang, BaoKai Wang, Arun Bansil, Horng-Tay Jeng, Titus Neupert, Adam Kaminski, Hsin Lin, Shuang Jia, and M. Zahid Hasan, "Discovery of a weyl fermion state with fermi arcs in niobium arsenide," Nature Physics **11**, 748 (2015).
[38] C. Zhang, Z. Yuan, S.-Y. Xu, Z. Lin, B. Tong, M. Z. Hasan, J. Wang, C. Zhang, and S. Jia, "Transport experiments: Tantalum monoarsenide: an exotic compensated semimetal," arXiv:1502.00251 (2015).
[39] Xiaochun Huang, Lingxiao Zhao, Yujia Long, Peipei Wang, Dong Chen, Zhanhai Yang, Hui Liang, Mianqi Xue, Hongming Weng, Zhong Fang, Xi Dai, and Genfu Chen, "Observation of the chiral-anomaly-induced negative magnetoresistance in 3d weyl semimetal taas," Phys. Rev. X **5**, 031023 (2015).
[40] Z. K. Liu, J. Jiang, B. Zhou, Z. J. Wang, Y. Zhang, H. M. Weng, D. Prabhakaran, S-K. Mo, H. Peng, P. Dudin, T. Kim, M. Hoesch, Z. Fang, X. Dai, Z. X. Shen, D. L. Feng, Z. Hussain, and Y. L. Chen, "A stable three-dimensional topological Dirac semimetal Cd3As2," Nat. Mater **13**, 677 (2014).
[41] Z. K. Liu, B. Zhou, Y. Zhang, Z. J. Wang, H. M. Weng, D. Prabhakaran, S.-K. Mo, Z. X. Shen, Z. Fang, X. Dai, Z. Hussain, and Y. L. Chen, "Discovery of a three-dimensional topological dirac semimetal, na3bi," Science (2014).
[42] Madhab Neupane, Su-Yang Xu, Raman Sankar, Nasser Alidoust, Guang Bian, Chang Liu, Ilya Belopolski, Tay-Rong Chang, Horng-Tay Jeng, Hsin Lin, *et al.*, "Observation of a three-dimensional topological dirac semimetal phase in high-mobility cd3as2," Nat. Comm. **5** (2014).
[43] L. P. He, X. C. Hong, J. K. Dong, J. Pan, Z. Zhang, J. Zhang, and S. Y. Li, "Quantum transport evidence for the three-dimensional dirac semimetal phase in cd_3as_2," Phys. Rev. Lett. **113**, 246402 (2014).
[44] Sangjun Jeon, Brian B. Zhou, Andras Gyenis, Benjamin E. Feldman, Itamar Kimchi, Andrew C. Potter, Quinn D. Gibson, Robert J. Cava, Ashvin Vishwanath, and Ali Yazdani, "Landau quantization and quasiparticle interference in the three-dimensional dirac semimetal cd3as2," Nature Materials **13**, 851 (2014).
[45] Su-Yang Xu, Chang Liu, Satya K Kushwaha, Raman Sankar, Jason W Krizan, Ilya Belopolski, Madhab Neupane, Guang Bian, Nasser Alidoust, Tay-Rong Chang, *et al.*, "Observation of fermi arc surface states in a topological metal," Science **347**, 294–298 (2015).
[46] Jun Xiong, Satya K. Kushwaha, Tian Liang, Jason W. Krizan, Max Hirschberger, Wudi Wang, R. J. Cava, and N. P. Ong, "Evidence for the chiral anomaly in the dirac semimetal na3bi," Science (2015), 10.1126/science.aac6089.
[47] Guang Bian, Tay-Rong Chang, Raman Sankar, Su-Yang Xu, Hao Zheng, Titus Neupert, Ching-Kai Chiu, Shin-Ming Huang, Guoqing Chang, Ilya Belopolski, Daniel S.Sanchez, Madhab Neupane, Nasser Alidoust, Chang Liu, BaoKai Wang, Chi-Cheng Lee, Horng-Tay Jeng, Arun Bansil, Fangcheng Chou, Hsin Lin, and M. Zahid Hasan, "Topological nodal-line fermions in the noncentrosymmetric superconductor compound pbtase2," arXiv:1505.03069 (2015).
[48] Andrew C. Potter, Itamar Kimchi, and Ashvin Vishwanath, "Quantum oscillations from surface fermi arcs in weyl and dirac semimetals," Nature Communications **5** (2014).
[49] Mehdi Kargarian, Mohit Randeria, and Yuan-Ming Lu, "Are the double fermi arcs of dirac semimetals topologically protected?" arXiv:1509.02180v1 (2015).
[50] J. Matsuno, K. Ihara, S. Yamamura, H. Wadati, K. Ishii, V. V. Shankar, Hae-Young Kee, and H. Takagi, "Engineering a spin-orbital magnetic insulator by tailoring superlattices," Phys. Rev. Lett. **114**, 247209 (2015).
[51] K. Knopp, *Theory of Functions Parts I and II, Two Volumes Bound as One, Part II* (Dover, 1996).
[52] M. E. Peskin, *An Introduction to Quantum Field Theory* (Westview Press, 1995).
[53] Siddharth A. Parameswaran, Ari M. Turner, Daniel P. Arovas, and Ashvin Vishwanath, "Topological order and absence of band insulaters at integer filling in nonsymmorphic crystals," Nature Physics **9**, 299 (2013).
[54] Daniel S. Freed and Gregory W. Moore, "Twisted equivariant matter," Annales Henri Poincare **14**, 1927 (2013).
[55] Chao-Xing Liu, Rui-Xing Zhang, and Brian K. VanLeeuwen, "Topological nonsymmorphic crystalline insu-

lators," Phys. Rev. B **90**, 085304 (2014).
[56] Chen Fang and Liang Fu, "New classes of three-dimensional topological crystalline insulators: Nonsymmorphic and magnetic," Phys. Rev. B **91**, 161105 (2015).
[57] Ken Shiozaki, Masatoshi Sato, and Kiyonori Gomi, "Z_2 topology in nonsymmorphic crystalline insulators: Möbius twist in surface states," Phys. Rev. B **91**, 155120 (2015).
[58] Dániel Varjas, Fernando de Juan, and Yuan-Ming Lu, "Bulk invariants and topological response in insulators and superconductors with nonsymmorphic symmetries," Phys. Rev. B **92**, 195116 (2015).
[59] Haruki Watanabe, Hoi Chun Po, Ashvin Vishwanath, and Michael P. Zaletel, "Filling constraints for spin-orbit coupled insulators in symmorphic and non-symmorphic crystals," arXiv:1505.04193 (2015).
[60] Ling Lu, Chen Fang, Liang Fu, Steven G Johnson, John D Joannopoulos, and Marin Soljačić, "Three-dimensional topological photonic crystal with a single surface dirac cone," arXiv preprint arXiv:1507.00337 (2015).
[61] Zhijun Wang, Aris Alexandradinata, Robert J. Cava, and B. Andrei Bernevig, "Hourglass fermions," in review (2015).
[62] H Kramers, "Th?rie g??ale de la rotation paramagn?ique daws lew cristaux," Proc. Amsterdam Akad. **33**, 959 (1930).
[63] Liang Fu and C. Kane, "Topological insulators with inversion symmetry," Phys. Rev. B **76**, 045302 (2007).
[64] G. Kress and J. Furthmuller, "Efficient iterative schemes for ab initio total-energy calculations using a plane-wave basis set," Phys. Rev. B **54**, 11169 (1996).
[65] J. P. Perdew, K. Burke, and M. Ernzerhof, "Generalized gradient approximation made simple," Phys. Rev. Lett. **77**, 3865 (1996).
[66] P. E. Blochl, "Projector augmented-wave method," Phys. Rev. B **50**, 17953 (1994).
[67] M. P. L. Sancho, J. M. L. Sancho, and J. Rubio, "Highly convergent schemes for the calculation of bulk and surface green functions," J. Phys. F: Met. Phys. **15**, 851 (1985).

Appendix A: Bulk invariant protected by $G*T$

1. Z_2 invariant protected by $G*T$

The bulk invariant is defined on a sphere in the Brillouin zone that encloses some band crossings (either nodal points or nodal lines), and on the surface of that sphere, the conduction and the valence bands have a finite direct gap and hence can be separated. For our case, due to Θ, the generic band crossing is either a pair of opposite Weyl points symmetric about XS or UR. We use a sphere centered at $\mathbf{k}_0$, a point on XS, with radius k_r. Each point on the sphere is parameterized by (θ, ϕ):

$$\begin{aligned}&(k_a, k_b, k_c) \\ &= (k_{0a} + k_r \cos\theta, k_{0b} + k_r \sin\theta\cos\phi, k_{0c} + k_r \sin\theta \sin\phi).\end{aligned} \tag{1}$$

The derivation of the Z_2 invariant on a sphere invariant under $\Theta = G*T$ closely follows the derivation of the Z_2 invariant of 2D topological insulators. (See Ref.[63].)

First we parameterize the sphere such that under Θ, a point at (θ, ϕ) is mapped to $(\theta, \phi+\pi)$. Since the total Chern number on the sphere vanish, and we can hence in principle choose a smooth gauge for all occupied bands, denoted by $|u_{n\in occ}(\theta,\phi)\rangle$. We can hence define the following sewing matrix

$$W_{mn}(\theta,\phi) = \langle u_m(\theta,\phi+\pi)|\Theta|u_n(\theta,\phi)\rangle. \tag{2}$$

At $\theta = 0, \pi$, we have

$$\begin{aligned}W_{mn}(0/\pi) &= \langle u_m(0/\pi)|\Theta|u_n(0/\pi)\rangle \\ &= (\langle \Theta u_m(0/\pi)|\Theta^2|u_n(0/\pi)\rangle)^2 \\ &= -\langle u_n(0/\pi)|\Theta|u_m(0/\pi)\rangle \\ &= -W_{nm}(0/\pi),\end{aligned} \tag{3}$$

i.e.,

$$W = -W^T(0/\pi). \tag{4}$$

Hence we can define the following Z_2 quantity

$$\delta_0 = \frac{\mathrm{Pf}[W(0)]}{\sqrt{\det[W(0)]}} \frac{\mathrm{Pf}[W(\pi)]}{\sqrt{\det[W(\pi)]}}, \tag{5}$$

where Pf stands for the Pfaffian of an antisymmetric matrix. Eq.(5) defines a Z_2 quantity which is either $+1$ or -1, because $\mathrm{Pf}^2 = \det$ in general.

To prove that the Z_2 quantity is also gauge invariant, consider changing the gauge by a smooth unitary N_{occ}-by-N_{occ} matrix $U(\theta,\phi)$

$$|u'_m(\theta,\phi)\rangle = \sum_n U_{mn}(\theta,\phi)|u_n(\theta,\phi)\rangle. \tag{6}$$

It is straight forward to see that after the transform, the sewing matrix becomes

$$W'(\theta,\phi) = U^T(\theta,\phi+\pi)W(\theta,\phi)U(\theta,\phi), \tag{7}$$

so that at $\theta = 0, \pi$

$$\begin{aligned}\mathrm{Pf}[W'(0/\pi)] &= \det[U(0/\pi)]\mathrm{Pf}[W(0/\pi)], \\ \det[W'(0/\pi)] &= \det[U^T(0/\pi)]\det[W(0/\pi)]\det[U(0/\pi)] \\ &= \det[W(0/\pi)]\det{}^2[U(0/\pi)].\end{aligned} \tag{8}$$

Substituting Eqs.(8) into Eq.(5), we find

$$\delta'_0 = \delta_0. \tag{9}$$

2. Simplification of the Z_2-invariant in spinful systems in the presence of inversion

In this section, we show how the Z_2-invariant given in terms of Pfaffians in Eq.(5) simplifies in the presence of inversion symmetry in a spinful system. In this section, we closely follow the derivation of the original Fu-Kane formula in topological insulators with inversion symmetry, which can be briefly summarized as follows: (i) the bands at time-reversal invariant momenta are also eigenstates of the inversion; (ii) each state and its time-reversal partner have the same inversion eigenvalue, so that each Kramers' pair at a TRIM maps to an eigenvalue of either $+1$ or -1; (iii) the product of the inversion eigenvalues of all occupied Kramers' pairs at all TRIM is the same as the Pffafian invariant.

In our case, the time-reversal symmetry is replaced by $\Theta = G*T$ and the points that are invariant under Θ are $\theta = 0, \pi$ on the sphere. The inversion symmetry itself is not a good quantum number at these points, but the composition symmetry $R_2 \equiv P*G$ is. We will now prove that for each degenerate pair of states at $\theta = 0, \pi$ have the same eigenvalue of R_2.

We distinguish two cases of (i) the inversion center is within the glide plane and (ii) the inversion center is not within the glide plane. A generic inversion operation takes the form

$$P:\ (x,y,z) \to (\frac{\lambda}{2} - x, \frac{\mu}{2} - y, \frac{\nu}{2} - z), \tag{10}$$

where $\lambda, \mu, \nu = 0, 1$. If $\lambda = 0$, then the inversion center, $(0, \mu, \nu)/2$ is on the glide plane; if $\lambda = 1$, then the inversion center $(1/2, \mu/2, \nu/2)$ is away from the glide plane.

If the inversion center is inside the glide plane, then we have

$$R_2:\ (x, \frac{\mu}{2} - y - \frac{1}{2}, \frac{\nu}{2} - z), \tag{11}$$

and

$$R_2^2 : (x,y,z). \tag{12}$$

Yet, since in spin space R^2 is equivalent to a full spin rotation, we have

$$R^2 = -1. \tag{13}$$

Also, the commutation relation between R_2 and Θ can be shown to be

$$R_2\Theta = T_{010}\Theta R_2 = e^{-ik_b}\Theta R_2. \tag{14}$$

From Eq.(13), each state at $\theta = 0, \pi$ is also an eigenstate of R_2 with eigenvalue of either $+i$ or $-i$. Using Eq.(14), we see that for each eigenstate of R_2 with eigenvalue $+i$

$$R_2\Theta|+i\rangle = e^{-ik_b}\Theta R_2|+i\rangle = -e^{-ik_b}i\Theta|+i\rangle, \quad (15)$$

i.e., $\Theta|+i\rangle$ is an eigenstate of R_2 with eigenvalue $-e^{-ik_b}i = +i$ at $\theta = 0, \pi$. Hence the two states in one degenerate pair at $\theta = 0, \pi$ have the same eigenvalue of R_2. Following Ref.[63], we show that the Z_2 invariant can be expressed in terms of these eigenvalues

$$\delta_0 = \prod_{n=1,\ldots,N_{occ}/2} \frac{\gamma_{2n}(0)}{\gamma_{2n}(\pi)}. \quad (16)$$

If the inversion center is away from the glide plane, we have

$$R_2 : (x + \frac{1}{2}, \frac{\mu}{2} - y - \frac{1}{2}, \frac{\nu}{2} - z), \quad (17)$$

which is in fact a twofold screw axis. The square of R_2 is

$$R_2^2 : (x + 1, y, z). \quad (18)$$

Again, considering the spin rotation in R_2, the eigenvalues are $\pm ie^{-ik_a/2}$ from Eq.(18). The commutation relation between R_2 and Θ is

$$R_2\Theta = T110\Theta R_2 = e^{-ik_a - ik_b}\Theta R_2, \quad (19)$$

so that for an eigenstate of R_2 with eigenvalue $+ie^{-ik_a/2}$, we have

$$R_2\Theta|+ie^{-ik_a/2}\rangle = -ie^{-ik_a/2-ik_b}|+ie^{-ik_a/2}\rangle. \quad (20)$$

Eq.(20) shows that at $\theta = 0, \pi$ (where $k_b = \pi$), the two degenerate states have the same eigenvalue of R_2. Therefore the following expression

$$\delta_0 = \prod_{n=1,\ldots,N_{occ}/2} \frac{e^{ik_0/2}\gamma_{2n}(0)}{e^{-ik_0/2}\gamma_{2n}(\pi)}. \quad (21)$$

Appendix B: Splitting of the nonsymmorphic Dirac point in the absence of inversion

In this section, we lift the symmetry of inversion, keeping glide reflection and time-reversal. Without the inversion, the bands are in general singly degenerate, and a single Dirac point splits into two Weyl points. Since glide reflection inverts the monopole charge of the Weyl point and time-reversal preserves it, the configuration of the split Dirac point is such that W_1 is related by W_2 by $\Theta = G * T$, while $W'_{1,2}$ are related to $W_{1,2}$ by time-reversal, in the presence of a inversion breaking perturbation. Yet it is important to note that even in this case, the system is not a generic Weyl semimetal, because each pair of Weyl points related by $G * T$, W_1 and W_2 for example, carry a Z_2 topological charge. Consider a sphere enclosing such a pair, and the definition of the Z_2 invariant only depends on the presence of $G * T$. Therefore, if this invariant is nontrivial in the presence of inversion due to the Dirac point, it remains nontrivial after the splitting. This Z_2 topological charge has two consequences: (i) on the surface preserving G, the Fermi arcs must *not* connect the projections of Weyl points that are related by $G * T$, and (ii) there must be an even number of such pairs of Weyl points due to the Nielson-Ninomiya theorem.

Appendix C: Some details of the numerics

The band structures of $(SrIrO_3)_{2m}(CaIrO_3)_{2n}$ are calculated in the framework of density functional theory (DFT) including the Hubbard U, as implemented in the Vienna *ab initio* simulation package (VASP) [64] by using generalized gradient approximation (GGA) of exchange-correlation function in the Perdew-Burke-Ernzerhof (PBE) form [65]. The projector augmented wave method [66] was applied to model the core electrons. Monkhorst-Pack **k**-point sampling of 4×4×2 was used for (m=1, n=1). Energy cutoff of the planewave basis was fully tested, and atomic structures were optimized with maximal residual forces smaller than 0.01 eV/Å. Spin-orbit coupling (SOC) was included in all calculations. For the Hubbard $U < 2$, all the results are similar, and here we only show the results for $U = 0$ for the sake of simplicity.

For $SrIrO_3$ (i.e. m=1, n=0), we got the similar results as the previous study[27], with Dirac nodal line around the Fermi energy. For $(SrIrO_3)_2(CaIrO_3)_2$, the Dirac nodal will fold around X point and is gapped expect a pair of Dirac points along XS since the two-fold screw symmetry is broken. The properties of band structure around the Dirac points of $(SrIrO_3)_2(CaIrO_3)_2$ can well described by adding some mass terms based on the TB model in Ref. [27].

The tight-binding model for $(SrIrO_3)_2(CaIrO_3)_2$ is

$$H = \begin{pmatrix} H_0 + H_1 & T + T_1 & 0 & e^{-ik_z}(T - T_1)^\dagger \\ (T + T_1)^\dagger & (H_0 - H_1)\epsilon + m_1 & T - T_1 & 0 \\ 0 & (T - T_1)^\dagger & H_0 + H_1 & T + T_1 \\ e^{ik_z}(T - T_1) & 0 & (T + T_1)^\dagger & H_0 - H_1 \end{pmatrix}$$

where $H_0 = 2t_p(\mathrm{cosk_x} + \mathrm{cosk_y})\tau_x$, $H_1 = (t_{1p}\mathrm{cosk_y} + \mathrm{t_{2p}cosk_x})\mathrm{s_y}\tau_y - (\mathrm{t_{1p}cosk_x} + \mathrm{t_{2p}cosk_y})\mathrm{s_x}\tau_y$, $T = t_p - it_d(\mathrm{sink_x s_y} +$

$\sin k_y s_x)\tau_y$, $T_1 = m_2(\sin k_x s_x + \sin k_y s_y)\tau_x$. By fitting with the DFT results, we can get the corresponding parameters, $t_p = -0.0785, t_d = 0.053, t_{1p} = -0.1331, t_{2p} = 0.1597, m_1 = 0.0112, m_2 = 0.0006, \epsilon = 0.3078$.

The surface band structures are calculated in an semi-infinite geometry by using the recursive Green's function method[67] based on the previous tight-binding model.